Interfacial Behavior of Block Polyelectrolytes. 6. Properties of Surface Micelles as a Function of R and X in P(S_{260}-*b*-VP_{240}/RX)

J. Zhu, A. Eisenberg,* and R. B. Lennox*

Department of Chemistry, McGill University, 801 Sherbrooke Street West, Montreal, Quebec, Canada H3A 2K6

Received December 26, 1991; Revised Manuscript Received June 11, 1992

ABSTRACT: The interfacial properties of AB diblock polyelectrolytes P(S_{260}-*b*-VP_{240}/RX), where PS = polystyrene, PVP = poly(4-vinylpyridinium), R = C_1 to C_{18}, and X = I and Br, have been studied in detail at the air–water interface using the Langmuir film balance technique. Previous studies[1,2] have been extended to explore the scope of the surface micellization phenomenon by varying the length of the pyridinium alkylating agent (R), studying the temperature dependence of surface pressure vs mean molecular area (i.e., π–A), and controlling the speciation and concentration of the counterion (Z^-) in the aqueous subphase. Surface micelle formation is a general phenomenon for all the materials measured, as shown using transmission electron microscopy (TEM) of the corresponding Langmuir–Blodgett (LB) films. It is shown that both the counterion and the hydrophobicity of R affect the relative balance between a surface micelle whose polyelectrolyte chains are surface-adsorbed (starfish morphology) and a surface micelle whose polyelectrolyte chains are subphase-solubilized (jellyfish morphology). Plateaus observed in π–A curves for diblocks with moderate to strong hydrophobic R groups are associated with a compression-induced solubilization of the alkylated polyelectrolyte chains. The balance between surface-adsorbed and solubilized PVP/R^+ chains can be readily altered by changing the counterion from Cl^- to Br^- to I^- or by changing the concentration of the counterion. The size, aggregation number, and conformation of the surface micelles derived from P(S_{260}-*b*-VP_{240}/RX) diblocks are shown to be readily tunable by a judicious choice of R, X, and the experimental conditions.

Introduction

The considerable interest in polymer monolayers arises because of both the technological applications of ultrathin polymer layers and the molecular details accessible in the monolayer experiment.[3–6] A number of materials have been shown to form relatively stable polymer monolayers at the air–wave interface, including polythiophenes, polyamides, etc.[7] We have recently been exploring aspects of the interfacial chemistry of block polyelectrolytes and, in particular, their monolayer-forming properties on aqueous surfaces.[1,2,7–9] These materials, made up of relatively monodisperse hydrophilic and hydrophilic/amphiphilic blocks, have been found to readily spread on water and form very stable monolayer films, while exhibiting a number of unusual features in their π–A isotherms including molecular weight dependences. With the aid of microscopy (transmission electron (TEM) and atomic force (AFM)) visualized Langmuir–Blodgett films of these materials, we have found that the monolayer films are, in fact, made up of a quasi-ordered array of self-assembled structures which we have termed *surface micelles*. These surface micelles form in the dilute surface concentration regime and assume morphologies (starfish, rods, extended planes, or sheets) which are dependent upon the balance between block sizes (ref 10; Figure 1).

The concept of surface micellization of amphiphiles was invoked by Langmuir in 1933 to rationalize the gas-analogous to condensed-analogous phase transition observed in low molecular weight amphiphiles.[11] Compared to these compounds, the block polyelectrolytes studied in our laboratories offer the advantages of having large adsorption free energies and of being directly observable by both electron and proximal probe microscopy techniques (i.e., TEM or AFM).

In a recent paper, we have studied the effects of varying the magnitudes and relative sizes of the two blocks.[2] In this study, we have extended our investigation of the surface micellization phenomenon by probing both the effect of altering the amphiphilic nature of the polyelectrolyte block and the effect of varying the electrolyte in the aqueous subphase. We show that the block polyelectrolyte surface micellization phenomenon has considerable generality and that the interfacial properties of these aggregates are readily "tunable" by a judicious choice of both the subphase conditions and diblock composition.

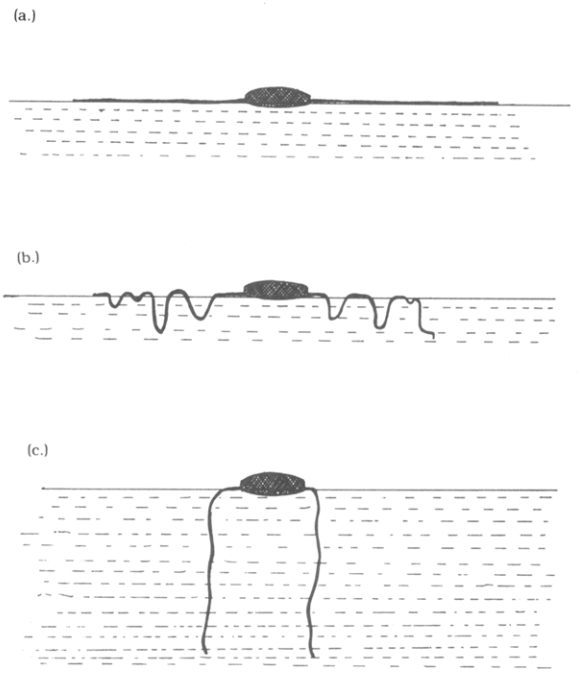

Figure 1. Schematic representation of (a) a starfish surface micelle, (b) a partially formed jellyfish surface micelle, and (c) a jellyfish surface micelle.

Experimental Section

Materials. The synthesis of P(S_{260}-*b*-VP_{240}) has been described elsewhere.[1] Quaternization was effected using methyl iodide, butyl iodide, hexyl iodide, decyl iodide, octadecyl iodide, and decyl bromide (all from Aldrich). The extent of quater-

* Authors to whom correspondence can be addressed.

0024-9297/92/2225-6556$03.00/0

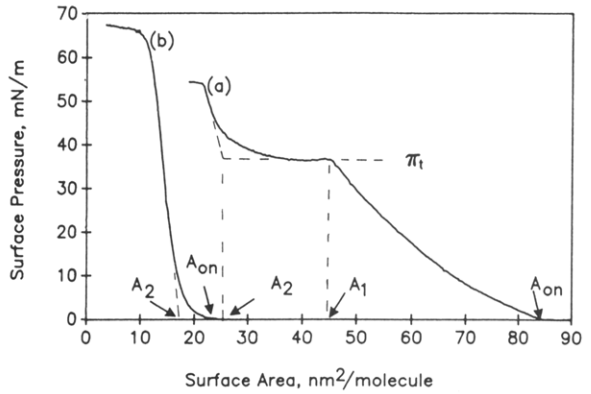

Figure 2. Schematic representation of area and surface pressure parameters associated with Langmuir films of the samples studied here.

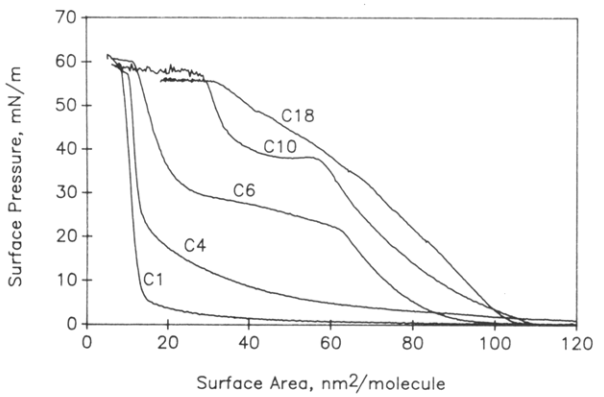

Figure 3. Surface pressure vs molecular area (π–A) curves for P(S_{260}-*b*-VP_{240}/RI) block polyelectrolytes on a pure water surface at 25 °C. R = methyl (C_1), *n*-butyl (C_4), *n*-hexyl (C_6), *n*-decyl (C_{10}), and *n*-octadecyl (C_{18}).

nization (~100% in all samples except for C_1, which was ~95%) was monitored by FTIR via the disappearance of the pyridine adsorption at 1414 cm^{-1}. NaCl, NaBr, KCl, and KI dissolved in the aqueous subphase were analytical grade from BDH and were vacuum oven-dried at 120 °C overnight before use.

Surface Balance Measurement and LB Films. As described previously,[1,2] a Langmuir film balance (Lauda Model D) was used to measure the surface pressure as a function of area (π–A) of polymer films spread from 0.5 mg/mL of polymer solution in a 4:1 mixture of chloroform/2-propanol. Deionized 18 MΩ (MilliQ, Toronto) water which had been passed through an organic residue cartridge was used throughout these studies. The compression rate was maintained at 15 mm/min. The experimental isotherm parameters A_{on}, A_1, A_2, and π_t are as indicated in Figure 2. Reference is made throughout the text to plateau and collapse pressures; the former refers to extended regions of the isotherms where $d\pi/dA \approx 0$, and the latter refers to the region of the isotherm where irreproducible discontinuities arise, i.e., at low A and high π.

LB films were transferred onto EM grids which had been precoated with Formvar and carbon at a present pressure under a constant vertical lifting speed of 1 mm/min. The LB films/EM grids were shadowed with platinum/palladium (60/40) at a low shadowing angle (15–20°) to provide contrast, and the transmission electron micrographs were acquired using a JEOL CX100-TEMSCAN electron microscope at 100 kV.

Results and Discussion

The π–A curves at 25 °C for P(S_{260}-*b*-VP_{240}/RI), where R = methyl, *n*-butyl, *n*-hexyl, *n*-decyl, and *n*-octadecyl, are shown in Figure 3. It is apparent that the isotherm parameters A_{on}, A_1, π_t, and A_2 are highly dependent upon the net hydrophobicity of the pyridinium alkylating group. General trends readily apparent from Figure 3 include

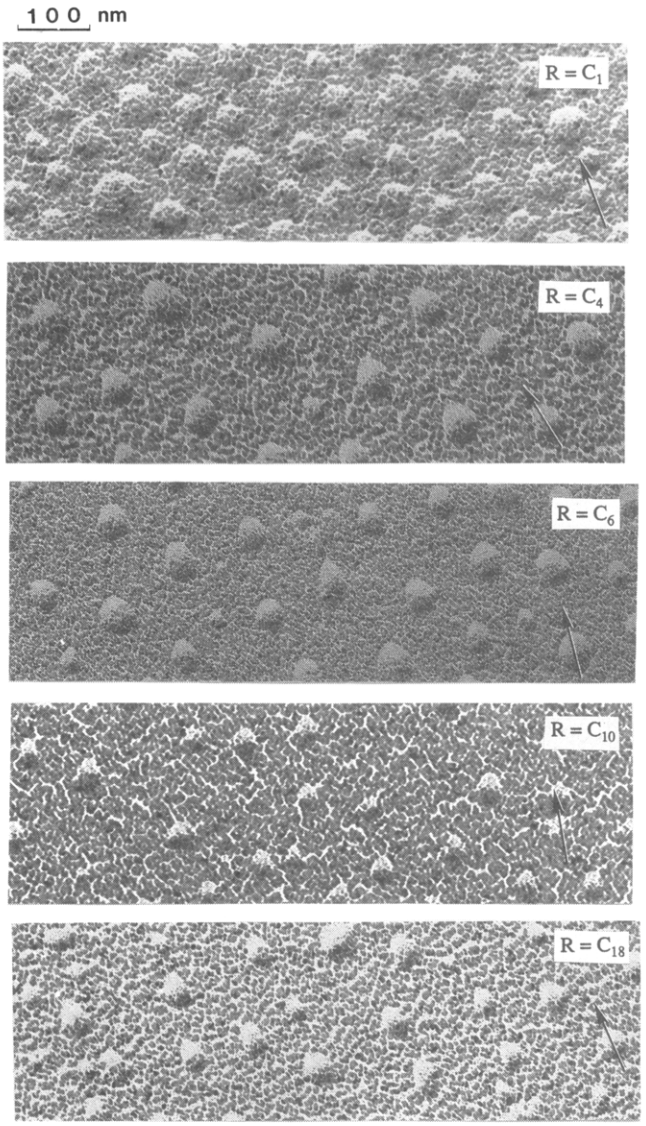

Figure 4. TEM photographs of P(S_{260}-*b*-VP_{240}/RI) LB films deposited on carbon-coated EM grids at π = 2 mN/m and shadowed with Pt/Pd (60/40) at a low angle (15–20°). R is as indicated in each photograph. The arrows indicate the direction of shadowing.

the following: (i) a distinct discontinuity in the isotherms for R ≥ C_6; (ii) plateau pressures, π_t, accompanying this discontinuity follow a trend of $C_6 < C_{10} < C_{18}$; (iii) the limiting area, A_2, follows the trend $C_1 < C_4 < C_6 < C_{10} < C_{18}$. The molecular origin of these trends and a description of the organizational states of the surface-adsorbed block ionomers are more readily discussed in conjunction with transmission electron microscopy images of the LB films (Figure 4) removed from the pure water surface. The temperature dependence of each sample is shown in Figure 5, and the effect of varying the speciation and concentration of the subphase electrolyte is shown in Figures 6–8.

Detailed insight into the organization and morphology of the monolayer-forming block polyelectrolytes is difficult if one relies exclusively on isotherm data. LB films have been examined to resolve this and to address the origin of unusual phenomena such as an abrupt onset of π, very flat, first-order-like plateaus, and a temperature inversion in the isotherms. We have made the assumption that a 1:1 correspondence exists between the organizational state of the Langmuir film and the deposited LB film. In other words, we assume that a distortionless transfer has occurred. Figure 4 shows the micrographs of each sample

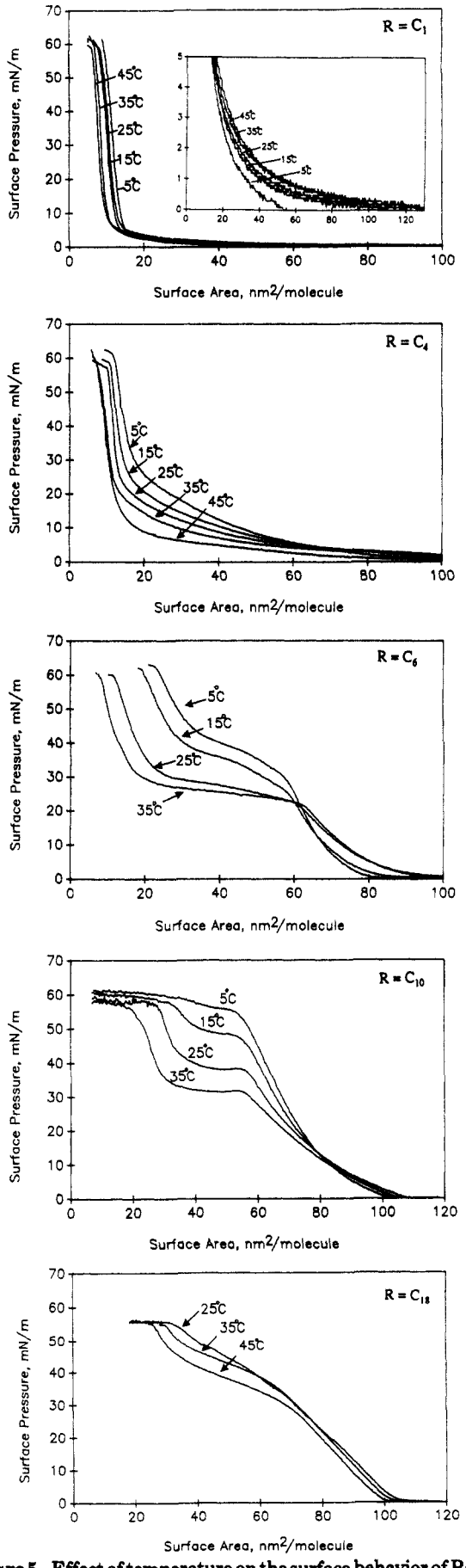

Figure 5. Effect of temperature on the surface behavior of P(S_{260}-*b*-VP_{240}/RI) block polyelectrolytes on pure water surface. R is as indicated in each figure.

(C_1 to C_{18}) deposited onto a carbon surface at 2 mN/m. Structures with uniform morphology (circular) and dimensions (diameter, center-to-center distances, height) are apparent in each case.

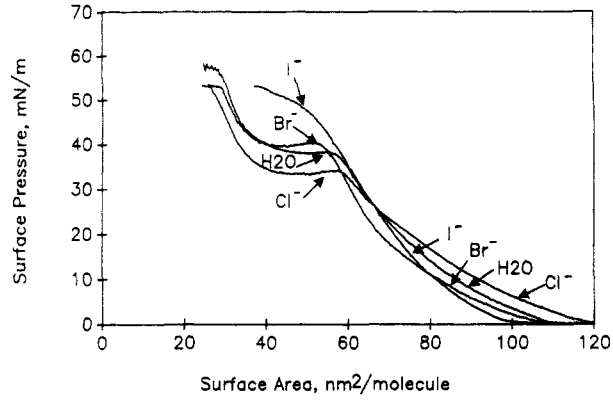

Figure 6. Effect of subphase electrolyte composition MX (0.1 N) on isotherms of P(S_{260}-*b*-VP_{240}/C_{10}I) at 25 °C. MX = KI, NaBr, and KCl. The isotherm on pure H_2O is provided for reference.

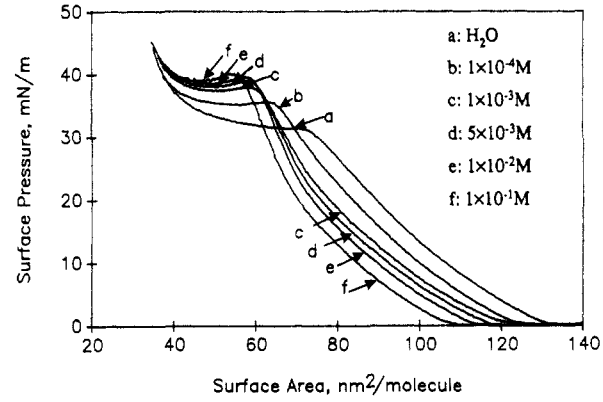

Figure 7. Effect of subphase salt concentration (NaBr) on isotherms of P(S_{260}-*b*-VP_{240}/C_{10}Br) block polyelectrolytes at 25 °C. Concentrations are as indicated.

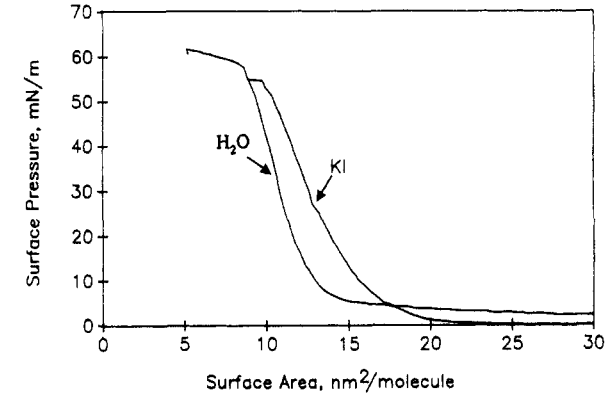

Figure 8. Isotherms of P(S_{260}-*b*-VP_{240}/C_1I) block polyelectrolytes on pure water and on 0.1 N KI at 25 °C.

An insight into the relationships between structure, surface morphology, molecular area, and surface pressure is accessible via a quantitative analysis of both the isotherms and electron micrographs. Previously, we have shown that the decylated material, P(S_{260}-*b*-VP_{240}/C_{10}I) block polyelectrolyte, forms highly regular aggregates at $\pi \geq 2$ mN/m.[1] To summarize earlier conclusions,[1,2] the C_{10} derivative forms aggregates which consist of a core of PS blocks and a corona of highly extended PVP/C_{10}I arms. These arms are entirely surface-adsorbed because of the hydrophobicity of the decyl chains. This state of the surface micelles is referred to as the starfish state (Figure 1). Decrease of the surface area on the film balance leads to an increase in the surface concentration of these species,

and at A_{on}, a measurable π results from the repulsive interactions of PVP/C_{10}I chains of adjacent surface micelles. Further compression leads to an interdigitation and lateral compression of the surface-adsorbed PVP/C_{10}I chains and also a flat to edge-on conformational change of the PVP rings. This conclusion is based on calculations of the area per VP at A_{on} and A_1 and comparison with the areas of a flat alkylated VP residue (ca. 0.48 nm^2, ref 20) and an edge-on residue (ca. 0.18 nm^2). The amount of remaining free water surface area is thus reduced on going from A_{on} to A_1. Further compression beyond A_1 forces the decylated PVP$^+$ moieties into the aqueous subphase. An alternative scenario wherein PVP/C_{10}I chains or segments extend out into the air is believed to be unlikely because it would be too energetically costly. The broad plateau corresponds to the incremental submersion of PVP/C_{10}I moieties until the subphase saturation concentration of PVP/C_{10}I has been reached. The monolayer at A_1 is thus made up of PS cores and PVP/C_{10}I chains adsorbed to the surface, with the C_{10} chains oriented upward into the air phase. The monolayer at areas greater than A_2 is highly incompressible due to repulsive PVP/C_{10}I–PVP/C_{10}I interactions and PS core/PS core incompressibility. The two extremes in morphology—the entirely surface-adsorbed micelle at $\pi < \pi_t$ and the structure where the ionic chains are for the most part subphase-dissolved—have been described as the "starfish" morphology and the "jellyfish" morphology, respectively.[1,2] The broad plateau is therefore termed a "starfish to jellyfish transition" and is π–A evidence for a molecular reorganization occurring in the monolayer.

R-Group Variation at 25 °C. The π–A curves obtained at 25 °C and their accompanying TEM's for the diblocks quaternized with other alkyl groups support this description and provide details regarding the relationship between the aggregation state, R group, and N_{Agg}. The C_{18}-alkylated material, for example, exhibits an A_{on} about the same as the C_{10} material (115 vs 109 nm/molecule) but a much higher π_t than the C_{10} material. In our model, A_{on} is directly related to the entire area excluded by the micelle's PS core and PVP/RX chains. The abrupt A_{on} is consistent with A_{on} originating from the interaction of preassembled molecules. If this were not the case, then surface reorganization would readily occur and a much more compressible film would be observed at low pressure. The plateau pressure, π_t, is very high (at least >55 mN/m) because the transition involves energetically costly solubilization of the VP/C_{18}I residues into the aqueous subphase. The π_t for the C_{18} material is higher than the C_{10} material by at least 20 mN/m, consistent with the considerably greater energy required to solubilize the C_{18} chains compared to the C_{10} chains. In summary, the C_{18} derivative's monolayer remains substantially two-dimensional even up to π = 50 mN/M because the quaternized VP residues are too hydrophobic to be solubilized at 25 °C. The LB electron micrographs support this general description, where at low pressure (π = 2 mN/m) rather uniform circular structures are observed with a surface density of >10^{10} particles/cm^2. Aggregation numbers of 70–90 and 80–130 are found for the C_{18} and C_{10} materials, respectively (Table I). The value of N_{Agg} for C_{18} is about 30% less than that measured for C_{10}, indicating that the aggregation phenomenon is at least partially controlled by the hydrophobicity of R. The net conclusion from this comparison is that C_{10} and C_{18} form similar types of surface micelles, except that the submerged polyelectrolyte state is a less favorable state for the C_{18} polymer than the C_{10} polymer.

Table I
Numerical Values for Surface Micelles of P(S_{260}-*b*-VP_{240}/RI) at π = 2 mN/m

	R = C_1	R = C_4	R = C_6	R = C_{10}	R = C_{18}
D (nm)[a]	45 ± 6	39 ± 5	37 ± 6	34 ± 5	30 ± 5
d (nm)[b]	77 ± 16	123 ± 22	113 ± 24	125 ± 28	102 ± 28
r (nm)[c]	16 ± 5	42 ± 13	38 ± 14	45 ± 17	36 ± 16
h (nm)[d]	8.9 ± 1.5	8.0 ± 1.2	7.7 ± 1.6	7.6 ± 1.5	6.8 ± 1.3

	calculated aggregation numbers (N_{Agg})				
method[e]	R = C_1	R = C_4	R = C_6	R = C_{10}	R = C_{18}
total area	143 ± 7	128 ± 4	156 ± 24	122 ± 3	86 ± 1
individual micelle area	193 ± 59	168 ± 53	123 ± 40	131 ± 35	84 ± 36
hexagonal lattice	153	132	125	131	89
PS volume[f]	248 ± 88	173 ± 57	151 ± 63	125 ± 51	91 ± 37
PS area	152 ± 40	111 ± 29	101 ± 32	83 ± 2	67 ± 22

[a] D = average diameter of PS cores. [b] d = average center-to-center distance between PS cores. [c] $r = (d - D)/2$; intercore distance. [d] h = height or thickness of the PS cores measured by metal shadowing. [e] Methods of calculating N_{Agg} from TEM's. For details, see ref 7. [f] Using h_e = 4 nm.[7]

The PVP/C_6I material exhibits a sharp rise in π at A_{on} as in C_{10} and C_{18} but a π_t which is substantially lower (23 vs 38 mN/m and >55 mN/m, respectively) and a plateau which is not horizontal. The lower π_t is consistent with the lower energy required for submersion of the less hydrophobic C_6-pyridinium moieties into the subphase. The sloping plateau at $\pi > \pi_t$ suggests the existence of more states than just a simple surface state and a pure submerged state. The finite solubility of C_6-pyridinium iodide in water suggests that many adjacent C_6-pyridinium residues can be simultaneously submerged to form loops in the subphase. The value of A_1 for the hexylated sample is, however, very similar to that of the C_{10} and C_{18} materials, consistent with the C_6 sample being entirely surface-adsorbed up to that point. The A_2 of the PVP/C_6I diblock is, however, considerably smaller than that of the PVP/C_{10}I diblock (i.e., 20 vs 36 nm^2/molecule), suggesting that the C_6 material forms a more complete jellyfish surface micelle (i.e., the polyelectrolyte chains are more completely submerged) than the C_{10} material at 25 °C (Figure 1). TEM's of the LB films of P(S_{260}-*b*-VP_{240}/C_6I) removed at 2 mN/m reveal circular micelles just as for the C_{10} and C_{18} derivatives. The core diameters are clearly larger than in the C_{10} and C_{18} cases, and the values of N_{Agg} (100–160) are correspondingly greater (Table I).

The PVP/C_4I material exhibits a large A_{on} (~230 nm^2/molecule), followed by a very broad, compressible region in the isotherm. At 25 °C, the isotherm appears to be quite simple, with large π values arising only at a small area per molecule. No distinct discontinuities are observed in this isotherm. TEM's of the material removed at 2 mN/m reveal that circular surface micelles form with this material as well; estimates of N_{Agg} range from 110 to 175 (Table I).

At 25 °C, the PVP/C_1I diblock material exhibits only very small surface pressures up to ca. 50 nm^2/molecule, consistent with the VP's not being surface-adsorbed. Furthermore, in the region where the film is quite incompressible, the areas correspond to area per VP values of 0.05–0.07 nm^2/VP residue. Such values are consistent with the polyelectrolyte chain adopting a conformation which extends into the subphase in some fashion (i.e., a jellyfish surface micelle; Figure 1). In agreement with previous measurements of P(MMA-*b*-VP/C_2Br) diblocks at the air–water interface,[16] we believe the PS coil in our work acts as a surface-adsorbed, water-insoluble buoy for the water-soluble PVP/C_1I chains. TEM's of a LB film

(2 mN/m) of PVP/C_1I exhibit a series of close-packed circular structures at high densities (ca. 10^{11} particles/cm^2). These structures show that surface micelles form even in the case of PVP/C_1I. Using the aggregation number determination techniques[8] once again, estimates of N_{Agg} range from 140 to 250, and the area of the PS core = 1.6 × 10^3 nm^2 or 6.1 nm^2 per PS block. The isotherm and LB film information allow one to conclude that the methylated material forms jellyfish surface micelles even at low π.

The high water solubility of PVP/C_1I and the fact that there is only very low surface pressure detectable at $A >$ 50 nm^2/molecule suggest that only aggregates whose PVP/C_1I chains are submerged are formed even at ~0 mN/m. The highly incompressible state which occurs soon after A_{on} is believed to be caused by repulsions between submerged VP chains on adjacent micelles. At π = 50 mN/m, for example, A = 12 nm^2/molecule, of which 6.1 nm^2 is attributable to the PS. The remaining 5.9 nm^2/molecule means that each VP/C_1 residue contributes 0.025 nm^2 to the projected area. Given that a fully extended PVP/C_1I chain would have a projected area of ~0.001 nm^2 per C_1 residue, it is clear that either the polyelectrolyte chains are not fully extended or chain–chain repulsions prevent denser packing.

Temperature Effects. Variation of the temperature between 5° and 45 °C produces marked changes for all the material studied. The C_{10} system has been previously discussed in detail.[1,2] To briefly summarize, the temperature dependence of both the plateau pressure and the A_2 value is believed to reflect the temperature dependence of the decylated polyelectrolyte solubilization process. At higher temperatures (i.e., 35 °C), the surface → subphase partitioning occurs more readily, and the final conformation at small areas is an almost completely developed jellyfish surface micelle. At lower temperatures (i.e., 15 °C), the solubilization process is less favorable, the π_t is larger, and the subphase solubility limit for PVP/C_{10}I chains at the interface is achieved. The result is evolution of a starfish micelle into a partial jellyfish.

A very similar series of isotherms is found for P(S_{260}-b-VP_{240}/C_6I) as for P(S_{260}-b-VP_{240}/C_{10}I). In this case, π_t decreases and the surface pressure in the A_{on} to A_1 region increases with increasing temperature. The A_2 values do not follow a smooth trend, however, with those at higher temperatures being less than those at lower temperatures. It appears that at higher temperatures, the surface-adsorbed polyelectrolyte becomes almost completely submerged at the point where π increases sharply (i.e., at areas less than A_2). At lower temperatures, the A_2 values are larger, suggesting that significant loop/train formation occurs. Temperature apparently serves to alter the balance between partial and complete submersion of the polyelectrolyte chains.

The PVP/C_4I material seems to exhibit properties of either complete or partial jellyfish surface micelles at large areas depending on the temperature. At higher temperatures (45 °C), the monolayer is highly compressible and has no plateau features; thus it appears to be in a jellyfish state throughout. A_2 values decrease on going from 5 to 25 °C, with the isotherms for 35 and 45 °C superimposable in the highly compressed state. These data are consistent with a complete jellyfish existing from A_{on} to the collapse region at 35–45 °C. At low temperatures, the PVP/C_4I chains contribute to the total area values even at high π, suggesting that some "partial jellyfish" state occurs. These temperature effects probably arise from the polyelectrolyte chain solubilization process.

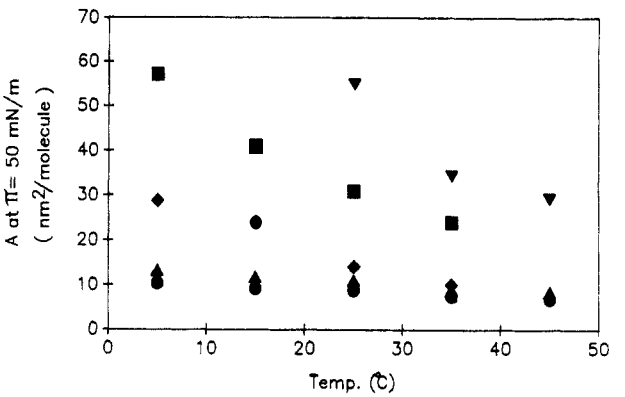

Figure 9. Plot of the mean molecular area at π = 50 mN/m as a function of temperature. R = C_1 (●), C_4 (▲), C_6 (♦), C_{10} (■), and C_{18} (▼).

The temperature dependence of the methylated material is consistent with the physical descriptions of the surface micelles provided above. Over the temperature range investigated, the isotherms retain the features of the 25 °C isotherm. No notable discontinuities are observed from A_{on} to A_2 but the value of A_2 progressively decreases with increasing temperature. Because the isotherm at even 5 °C has no features associated with surface-adsorbed polyelectrolyte chains, it is apparent that at temperatures higher than 5 °C, the PVP/C_1 chains are completely solubilized (i.e., the micelle is in a jellyfish state) and the dominant factors contributing to the surface area at high π are the interactions between surface-adsorbed PS cores and between PVP^+ chains.

An additional perspective on the temperature dependence is available from Figure 9. A plot of the area at high surface pressure (π = 50 mN/m) against temperature clearly shows the differences that exist with materials which readily adopt a jellyfish conformation and those which do not. The C_1 and C_4 materials have both a very small area and temperature dependence at high π values, consistent with the expected propeties of a well-formed jellyfish micelle. P(S_{260}-b-VP_{240}/C_6I), however, does not achieve the same area as the C_1 and C_4 derivatives until the subphase temperature is ~40 °C. The C_{10} and C_{18} derivatives are clearly far from the complete jellyfish state at 35 °C but evidently will approach it at much higher temperatures. The C_{10} and C_{18} derivatives are quite compressible at low temperatures but become highly condensed at elevated temperatures. This is consistent with the jellyfish state being possible at high temperatures.

Electrolyte Effects. The experimental variation of subphase electrolyte has focused primarily on the P(S_{260}-b-VP_{240}/C_{10}X) material. First, both the cation and anion of the subphase electrolyte MZ have been varied. Changing M^+ from N^+ to K^+ (Z^- = Cl^-) leads to no change in the isotherms. Changing Z^- (I^-, Br^-, Cl^-), however, causes large changes in the isotherms for P(S_{260}-b-VP_{240}/C_{10}I). A_{on} and A_1 values consistently decrease, and π_t values increase on going from X^- = Cl^- to Br^- to I^-. The resulting isotherms therefore feature lower pressures at areas less than A_1 for I^- than Cl^- and greater pressures at areas larger than A_1 for I^- than Cl^-. These trends are consistent with the compression-induced reorganization of the polyelectrolyte chains for the following reasons. The equilibrium

$$X^- + VP^+/R \overset{K_x}{\rightleftarrows} VP/RX \qquad (1)$$

is known to follow the trend $K_I > K_{Br} > K_{Cl}$ for PVP/R^+ homopolymers at the air–water interface.[17] Paralleling this binding strength series is the readily observed

insolubility of long-chain alkylpyridinium iodides in water compared with the substantial solubility of the corresponding chlorides. The trend in A_{on} values suggests that initial micelle interactions occur at a smaller area with I^- < Br^- < Cl^-. This in turn suggests that in the I^- case, radially oriented polyelectrolyte chains are less highly extended than in the Cl^- case. Stronger binding by I^- leads to a higher proportion of VP/R^+ residues being effectively neutralized, which in turn slightly reduces the extent of chain-elongating intramolecular electrostatic repulsions compared to the Cl^- case. The difference between A_{on} and A_1 in these three isotherms is quite constant (60–65 nm^2/molecule) for each salt species, despite the substantial difference in the actual values of A_{on} and A_1. This suggests that the polyelectrolyte chain–chain interpenetration and VP^+ ring reorientation (i.e., flat to edge-on) processes involve the same area contraction whether the polyelectrolyte chain is highly or only moderately charged. This condition in turn will arise only if the polyelectrolyte chain assumes a purely 2D conformation on the surface and does not extend into a third dimension (i.e., the subphase or air) while in the A_{on} to A_1 region of the isotherm. These data therefore further support our contention that the $A_{on} \rightarrow A_1$ region is related to the properties of *surface-adsorbed* polyelectrolyte chains.

The trends in π_t as a function of electrolyte reflect both the stability of the "starfish" micelles whose polyelectrolyte chains are interpenetrated and the degrees of difficulty in solubilizing the $VP/C_{10}{}^+X^-$ ion pairs in the subphase. At a given MX concentration, the degree of dissociation (α) follows the trend $\alpha_{Cl^-} > \alpha_{Br^-} > \alpha_{I^-}$.[17] Given that $VP^+/C_{10}X^-$ tight ion pairs will have limited water solubility and thus will tend to remain on the water surface, the compression-induced solubilization process will be more difficult for the I^--containing case. A quantitative relationship between π_t and α is not presently accessible because we do not have accurate values of the ion exchange constants between surface-adsorbed VP/R^+I^- and externally added Br^- and Cl^-.

Changing the subphase salt concentration (i.e., NaBr with $P(S_{260}\text{-}b\text{-}VP_{240}/C_{10}Br)$) produces significant changes in the isotherms, with values of A_{on} and A_1 decreasing and π_t increasing with increasing NaBr concentration. Because the polyelectrolyte ions are initially in the bromide form, the complications caused by ion exchange selectivity are avoided. The difference between A_{on} and A_1 (i.e., the lead-up to the plateau) remains reasonably constant (60 nm^2/molecule) at low concentrations of NaBr, with a decrease observed on going to higher salt concentrations (55 nm^2/molecule for 0.01 M NaBr, 53 nm^2/molecule for 0.1 M NaBr). This trend suggests that the salt induces subtle changes in the PVP chain dimensions. Such chain dimension changes also explain why A_{on} decreases with increasing salt and why the apparent free surface area at A_{on} is reduced at high salt concentration. The π_t trend reflects the ion pair equilibrium constant (K_X), with a higher concentration of X^- leading to a higher proportion of tight ion pairs being formed. These ion pair are, in turn, more difficult to solubilize in the subphase than the loose, solvent-separated ion pairs and lead to elevated π_t values. Because the maximum salt concentration is relatively modest (0.1 M), the apparent differences are negligible between a γ vs A and π vs A[18] representation of the data. The large monolayer expansion effects observed at low salt concentration are therefore believed to be real and are not artifacts of data presentation.

Table II
Data Associated with $P(S_{260}\text{-}b\text{-}VP_{240}/C_{10}Br)$ on $NaBr\text{–}H_2O$ at 25 °C

[NaBr] (M)	A_{on}[a]	A_1[a]	$(A_{on} - A_1)$[b]	W_1[c]	W_2[c]	π_t[d]
0	132	73	59	470	635	31.7
1×10^{-4}	125	65	60	525	550	35.4
1×10^{-3}	121	61	60	525	525	37.8
5×10^{-3}	119	60	59	500	535	38.9
1×10^{-2}	115	60	55	475	530	39.4
1×10^{-1}	110	57	53	440	485	40.0

[a] Units of nm^2/molecule. [b] Difference in mean molecular areas between A_{on} and A_1. [c] W_1 and W_2 are the values of the work calculated from areas under π–A curves from A_{on} to A_1 and from A_1 to A_2, respectively. Units of $kJ \cdot mol^{-1}$. [d] Plateau pressure at A_1. Units of mN/m.

Further insight into the polyeletrolyte chain reorientation process from A_{on} to A_1 and from A_1 to A_2 can be gleaned from considering the area under the π–A curve between these limits, as it is related to the work done on the film during compression (Table II). In the A_{on} to A_1 region, increasing the salt concentration has no effect on the work done; evidently electrostatic effects on the surface-adsorbed chains are not particularly significant. In the A_1 to A_2 (i.e., the plateau region) region, however, the work required to solubilize the chains is greater with more salt present. This is because of the solubility phenomenon described above and, perhaps, because of osmotic pressure factors.[19]

At the present time, the linking of electrolyte effects to surface $\rightleftharpoons$ subphase partitioning and polyelectrolyte chain dimension changes provide the most self-consistent description of the system. Models of electrolyte/charged monolayer interactions predict a variety of $\pi = f([X^-])$ relationships,[20,21] none of which are adhered to for the data in Figure 7. If the foregoing description of the process occurring in the A_{on} to A_1 region is valid, then a lack of adherence to those models is not surprising. The subtleties arising in this system, such as the nature of electrostatic effects of prone vs edge-on VP/R^+ rings and backbone reorientation, require more complex modeling conditions than are inherent in previous approaches.[20,21]

For the methylated material, as shown in Figure 8, subphase 0.1 N KI greatly reduces the values of A_{on} (22 nm^2/molecule with KI vs 130 nm^2/molecule for pure H_2O) and expands the condensed phase. Both changes are consistent with this material existing in a jellyfish state. Specific I-binding (loose or tight) to the solubilized $VP/C_1{}^+$ residues will reduce the overall chain–chain electrostatic repulsions by reducing the net effective charge on each chain. Moreover, the high electrolyte concentration will screen the fixed cationic charges, resulting in a significant lessening of chain–chain repulsions. The differences in the two isotherms at high compression may reflect a combination of increased polyelectrolyte chain coiling in the added KI case and retention of a highly extended polyelectrolyte chain conformation in the pure H_2O subphase case.

Summary

These studies have shown that surface micellization and self-assembly of $P(S_{260}\text{-}b\text{-}VP_{240}/RX)$ is a very general phenomenon and that the distinct plateau observed in π–A isotherms is diagnostic of the orientation of the polyelectroyte chains. The hydrophobicity of the quaternization agent, R, determines whether the polyelectrolyte chains are surface-adsorbed or are submerged at a low surface concentration of the polymer. In one extreme, the C_{10} and C_{18} derivatives form surface micelles at low

π where the PS blocks aggregate to form a circular "core" and the PVP/R^+ chains assume a radial, 2D orientation from this core. These chains are almost entirely surface-adsorbed at low π. In the other extreme, the PS blocks of the C_1 derivative also aggregate to form a circular core but the polyelectroyte PVP/C_1^+ chains, being very water soluble, assume a subphase conformation approximately perpendicular to the interface. The surface micellization phenomenon is clearly driven by PS–PS interactions, and the aggregate size is influenced by the hydrophobicity of R. Electrolyte effects on isotherm features are pronounced and reflect significant solubility changes and small electrostatic effects in the R = C_{10} case and measurable electrostatic effects in the R = C_1 case. In this regard, both the composition and concentration of the electrolyte provide ready control over chain–chain interactions by affecting inter- and intramolecular interactions. In the latter case, extended chain $\rightleftarrows$ coil conformational changes appear to be manifested in isotherm features of the C_1 material. The film balance experiment may therefore be useful as a very sensitive means to probe chain–chain interactions in 2D and 3D and may provide an important adjunct to surface force apparatus measurements between polymer brushes.[22]

Acknowledgment. Financial support of this research from NSERC (Canada) (R.B.L. and A.E.) is gratefully ackowledged.

References and Notes

(1) Zhu, J.; Eisenberg, A.; Lennox, R. B. *J. Am. Chem. Soc.* **1991**, *113*, 5583.
(2) Zhu, J.; Eisenberg, A.; Lennox, R. B. *Macromolecules*, previous paper in this issue.
(3) (a) Crisp, D. J. *Surface Phenomena in Chemistry and Biology*; Danielli, J. F., Pankhurst, K. G. A., Riddiford, A. C., Eds.; Pergamon: London, 1958. (b) Crisp, D. J. *J. Colloid Sci.* **1946**, *1*, 49, 161.
(4) Kim, M. W.; Chung, T. C. *J. Colloid. Interface Sci.* **1988**, *124*, 365.
(5) Brinkhuis, R. H. G.; Schouten, A. J. *Macromolecules* **1991**, *24*, 1496.
(6) Yu, H.; Sauer, B. B. *Macromolecules* **1987**, *20*, 393.
(7) (a) Ahmed, F. R.; Wilson, E. G.; Moss, G. P. *Thin Solids Films* **1990**, *187*, 141. (b) Gaines, G. L. *Langmuir* **1991**, *7*, 834.
(8) Zhu, J.; Lennox, R. B.; Eisenberg, A. *Langmuir* **1991**, *7*, 1579.
(9) Zhu, J.; Eisenberg, A.; Lennox, R. B. *Makromol. Chem.* **1992**, *53*, 211.
(10) Zhu, J.; Lennox, R. B.; Eisenberg, A. *J. Phys. Chem.* **1992**, *96*, 4727.
(11) Langmuir, I. *J. Chem. Phys.* **1933**, *1*, 756.
(12) Middleton, S. R.; Iwahashi, M.; Pallas, N. R.; Pethica, B. A. *Proc. R. Soc. London* **1984**, *396*, 143.
(13) Duda, G.; Schouten, A. J.; Arndt, T.; Lieser, G.; Schmidt, G. F.; Bubeck, C.; Wegner, G. *Thin Solid Films* **1988**, *159*, 221.
(14) Biegajski, J. E.; Cadenhead, D. A.; Prasad, P. N. *Langmuir* **1988**, *4*, 689.
(15) Kawaguchi, T.; Nakahara, H.; Fukoda, K. *Thin Solid Films* **1989**, *155*, 29.
(16) Bringuier, E.; Vilanove, R.; Gallot, Y.; Selb, J.; Rondelez, F. *J. Colloid Interface Sci.* **1985**, *104*, 95.
(17) Plaisance, M.; Ter-Minassian-Saraga, L. *J. Colloid Interface Sci.* **1976**, *56*, 33.
(18) Aston, M. S.; Herrington, J. M. *J. Colloid Interface Sci.* **1991**, *141*, 50.
(19) Granick, S.; Herz, J. *Macromolecules* **1985**, *18*, 460.
(20) Kawaguchi, M.; Itoh, S.; Takahashi, A. *Macromolecules* **1987**, *20*, 1052.
(21) Bringuier, E. *J. Phys. (Paris), Lett.* **1984**, *45*, 107.
(22) Milner, S. T. *Science* **1991**, *251*, 905.